









# Excited-state absorption and upconversion pumping of $\text{Tm}^{3+}$ -doped potassium lutetium double tungstate

ALEKSEY TYAZHEV,<sup>1</sup>  PAVEL LOIKO,<sup>2</sup> LAUREN GUILLEMOT,<sup>2</sup>   
ALEXANDRE KOUTA,<sup>1</sup> ROSA MARIA SOLÉ,<sup>3</sup>  XAVIER MATEOS,<sup>3</sup>   
MAGDALENA AGUILÓ,<sup>3</sup> FRANCESC DÍAZ,<sup>3</sup> HIPPOLYTE DUPONT,<sup>4</sup>  
PATRICK GEORGES,<sup>4</sup>  FRÉDÉRIC DRUON,<sup>4</sup>  ALAIN BRAUD,<sup>2</sup>  
PATRICE CAMY,<sup>2</sup> AND AMMAR HIDEUR<sup>1,\*</sup>

<sup>1</sup>CORIA UMR6614, CNRS-INSA-Université de Rouen, Normandie Université, Avenue de l'université, BP. 12, 76801 Saint Etienne du Rouvray, France

<sup>2</sup>Centre de Recherche sur les Ions, les Matériaux et la Photonique (CIMAP), UMR 6252 CEA-CNRS-ENSICAEN, Université de Caen Normandie, 6 Boulevard Maréchal Juin, 14050 Caen Cedex 4, France

<sup>3</sup>Física i Cristal·Lografia de Materials (FiCMA), Universitat Rovira i Virgili (URV), 43007 Tarragona, Spain

<sup>4</sup>Université Paris-Saclay, Institut d'Optique Graduate School, CNRS, Laboratoire Charles Fabry, 91127 Palaiseau, France

\*hideur@coria.fr

**Abstract:** We report on a bulk thulium laser operating on the  ${}^3\text{H}_4 \rightarrow {}^3\text{H}_5$  transition with pure upconversion pumping at 1064 nm by an ytterbium fiber laser (addressing the  ${}^3\text{F}_4 \rightarrow {}^3\text{F}_{2,3}$  excited-state absorption (ESA) transition of  $\text{Tm}^{3+}$  ions) generating 433 mW at 2291 nm with a slope efficiency of 7.4% / 33.2% vs. the incident / absorbed pump power, respectively, and linear laser polarization representing the highest output power ever extracted from any bulk 2.3  $\mu\text{m}$  thulium laser with upconversion pumping. As a gain material, a  $\text{Tm}^{3+}$ -doped potassium lutetium double tungstate crystal is employed. The polarized ESA spectra of this material in the near-infrared are measured by the pump-probe method. The possible benefits of dual-wavelength pumping at 0.79 and 1.06  $\mu\text{m}$  are also explored, indicating a positive effect of co-pumping at 0.79  $\mu\text{m}$  on reducing the threshold pump power for upconversion pumping.

© 2023 Optica Publishing Group under the terms of the [Optica Open Access Publishing Agreement](#)

## 1. Introduction

Excited-state absorption (ESA) is a process of excitation of an ion from a lower-lying excited-state to a higher-lying one with absorption of a photon [1,2]. For rare-earth ions ( $\text{RE}^{3+}$ ) frequently possessing a ladder-like energy-level structure, resonant ESA at the pump or laser wavelengths is rather probable while it is usually considered as a detrimental effect as it causes additional energy losses leading to a reduction in the slope efficiency or even laser ceasing. However, ESA can also serve as a key process for upconversion (UC) pumping schemes where two or more pump photons are used to populate a higher-lying excited-state of a  $\text{RE}^{3+}$  ion leading to Stokes or anti-Stokes emission from this manifold [3–5]. Usually, UC pumping is employed to achieve emission of visible laser photons while pumping in the near-infrared (an anti-Stokes process). It has been demonstrated for several  $\text{RE}^{3+}$  ions such as  $\text{Er}^{3+}$  [6],  $\text{Nd}^{3+}$  [7],  $\text{Tm}^{3+}$  [5,8] and  $\text{Pr}^{3+}$  [9].

Thulium ( $\text{Tm}^{3+}$ ) ions possess an electronic configuration of  $[\text{Xe}]4f^{12}$  with a ground-state  ${}^3\text{H}_6$  and a long-living first excited-state  ${}^3\text{F}_4$ . They are well-known for the  ${}^3\text{F}_4 \rightarrow {}^3\text{H}_6$  laser transition corresponding to emission around 2  $\mu\text{m}$  [10,11]. They also offer a possibility to generate light at yet longer wavelengths, at 2.3  $\mu\text{m}$ , due to the  ${}^3\text{H}_4 \rightarrow {}^3\text{H}_5$  transition [12]. 2.3  $\mu\text{m}$  Tm lasers are of

practical importance for gas sensing in the atmosphere, see Fig. 1, non-invasive glucose blood measurements and (potentially) pumping of mid-infrared optical parametric oscillators based on non-oxide crystals.

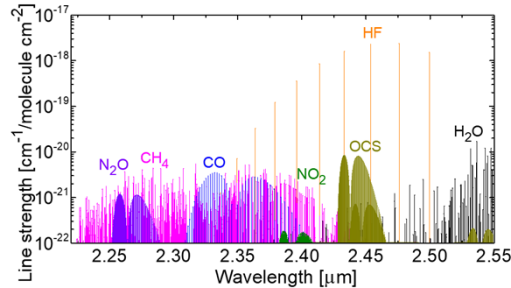


**Fig. 1.** HITRAN (spectroscopic database) simulation of absorption of molecular species in the spectral range covered by the  ${}^3\text{H}_4 \rightarrow {}^3\text{H}_5$  emission of thulium ions [13].

There are several difficulties to achieve laser emission at  $2.3\ \mu\text{m}$  using  $\text{Tm}^{3+}$  ions: (i) a fast quenching of the upper laser level ( ${}^3\text{H}_4$ ) lifetime by a cross-relaxation (CR) process,  $\text{Tm}_1({}^3\text{H}_4) + \text{Tm}_2({}^3\text{H}_6) \rightarrow \text{Tm}_1({}^3\text{F}_4) + \text{Tm}_2({}^3\text{F}_4)$  which is efficient even at moderate  $\text{Tm}^{3+}$  doping levels, (ii) a non-negligible multiphonon non-radiative (NR) relaxation from the  ${}^3\text{H}_4$   $\text{Tm}^{3+}$  level, especially in oxide matrices, and (iii) a strong competition with the high-gain  ${}^3\text{F}_4 \rightarrow {}^3\text{H}_6$  transition [14], Fig. 2. The advantage of the  ${}^3\text{H}_4 \rightarrow {}^3\text{H}_5$  transition with respect to similar transitions of other rare-earth ions ( $\text{Er}^{3+}$  or  $\text{Ho}^{3+}$ ) is that the terminal laser level ( ${}^3\text{H}_5$ ) is fast quenched by the NR relaxation thus avoiding the bottleneck effect. Consequently, continuous-wave (CW) laser operation at  $2.3\ \mu\text{m}$  is readily achieved [15–17]. It was demonstrated that an energy-transfer upconversion (ETU) process from the metastable  ${}^3\text{F}_4$   $\text{Tm}^{3+}$  state,  $\text{Tm}_1({}^3\text{F}_4) + \text{Tm}_2({}^3\text{F}_4) \rightarrow \text{Tm}_1({}^3\text{H}_4) + \text{Tm}_2({}^3\text{H}_6)$  acting opposite to the CR process and refilling the upper laser level may help to increase the laser slope efficiency above the Stokes limit [14].

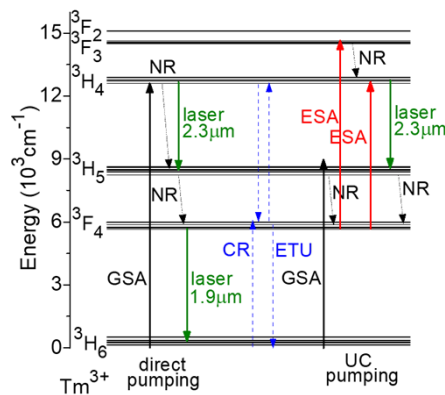


**Fig. 2.** A partial energy-level scheme of  $\text{Tm}^{3+}$  ions in potassium lutetium double tungstate [18] showing processes relevant for  $2.3\ \mu\text{m}$  laser operation: GSA / ESA – ground / excited state absorption, CR – cross-relaxation, ETU – energy-transfer upconversion, green arrows – laser transitions, NR – multiphonon non-radiative relaxation.

Recently, an UC pumping scheme was proposed for thulium ( $\text{Tm}^{3+}$ ) ions [19] targeting its laser transition  ${}^3\text{H}_4 \rightarrow {}^3\text{H}_5$ , Fig. 2. It is based on a combination of a weak phonon-assisted ground-state absorption (GSA)  ${}^3\text{H}_6 \rightarrow {}^3\text{H}_5 + h\nu_{\text{ph}}$  and a resonant ESA from the metastable  $\text{Tm}^{3+}$  state,  ${}^3\text{F}_4 \rightarrow$

$^3F_{2,3}$ , and its efficiency is boosted by a photon avalanche mechanism [20]. The main interest in pursuing this UC pumping scheme is the possibility to employ commercial, high-brightness and power-scalable Yb-fiber lasers (YFLs) emitting above 1  $\mu\text{m}$  as pump sources of 2.3  $\mu\text{m}$  Tm lasers. The high pump beam quality is essential for the development of femtosecond mode-locked (ML) lasers or waveguide lasers. Currently, ML Tm lasers operating on the  $^3H_4 \rightarrow ^3H_5$  transition are usually pumped by expensive and complex Ti:Sapphire lasers [21,22].

The recent progress on bulk and fiber Tm lasers operating on the  $^3H_4 \rightarrow ^3H_5$  transition with UC pumping slightly above 1  $\mu\text{m}$  is summarized in Table 1. Guillemot *et al.* first reported on a bulk Tm:LiYF<sub>4</sub> laser pumped by a Ti:Sapphire laser tuned to 1040 nm, almost to the extreme of its tunability curve, generating 102 mW at 2.30  $\mu\text{m}$  with a slope efficiency  $\eta$  of 14.6% [19]. Morova *et al.* employed a commercial 1064 nm YFL for UC pumping of a Tm:KY<sub>3</sub>F<sub>10</sub> laser whilst leading to a marginal power scaling to 124 mW at 2.34  $\mu\text{m}$  with a lower  $\eta$  of 8% [23]. Superior results were achieved in the fiber laser geometry: Tyazhev *et al.* reported on a Tm:ZBLAN fiber laser UC pumped by a home-made YFL tuned to 1049 nm delivering 1.24 W at 2.28  $\mu\text{m}$  with a slope efficiency  $\eta$  of 37.0% [25].

**Table 1. Output Characteristics<sup>a</sup> of Upconversion Pumped ~2.3  $\mu\text{m}$  Tm Lasers Reported So Far**

Material	Pump <sup>b</sup>	$\lambda_p$ , nm	$P_{th}$ , W	$P_{out}$ , mW	$\eta$ , %	$\lambda_L$ , $\mu\text{m}$	Ref.
<i>Bulk lasers</i>							
Tm:LiYF <sub>4</sub>	TS	1040	0.21	102	<b>14.6<sup>Inc</sup></b>	2.30	[19]
	TS	1055	0.31	46	10.9 <sup>Inc</sup>	2.30	[19]
Tm:KY <sub>3</sub> F <sub>10</sub>	TS	1048	0.34	92	14 <sup>Inc</sup>	2.27, 2.33	[17]
	YFL	1064	~0.80	124	8 <sup>Inc</sup>	2.34	[23]
Tm:KLu(WO <sub>4</sub> ) <sub>2</sub>	YFL	1064	3.19	<b>433</b>	7.4 <sup>Inc</sup>	2.29	This work
<i>Fiber lasers</i>							
Tm:ZBLAN	NL	1064	0.70	150	<b>7.8<sup>Inc</sup></b>	2.31	[24]
Tm:ZBLAN	YFL	1049	0.60	<b>1240</b>	<b>37.0<sup>Inc</sup></b>	2.28	[25]

<sup>a</sup> $\lambda_p$  – pump wavelength,  $P_{th}$  – laser threshold,  $P_{out}$  – output power,  $\eta$  – slope efficiency (*Inc* - vs. incident pump power),  $\lambda_L$  – laser wavelength.

<sup>b</sup>TS – Ti:Sapphire laser, NL – bulk Nd:YAG laser, YFL – ytterbium fiber laser.

Consequently, so far, the potential of UC pumping of bulk 2.3  $\mu\text{m}$  thulium lasers relying on the Yb-fiber laser technology was not fully exploited. In the present work, we aimed to demonstrate a power-scalable UC pumped bulk thulium laser at 2.3  $\mu\text{m}$ . For this, we employed a monoclinic crystal of potassium lutetium double tungstate (KLu(WO<sub>4</sub>)<sub>2</sub>) doped with Tm<sup>3+</sup> ions [26]. This crystal is a well-known gain medium for lasers at ~2  $\mu\text{m}$  [27–29]. Its particular feature is the strong polarization anisotropy of transition cross-sections originating from the low site symmetry ( $C_2$ ) for the dopant ions. The ESA spectra of Tm<sup>3+</sup> ions in this material have never been reported. Our hypothesis was that high ESA cross-sections can be attained with this material for specific light polarizations. Thus, this work also involved an ESA study.

## 2. Excited-state absorption

### 2.1. Crystal growth

The studied laser material was grown by the Top-Seeded Solution Growth Slow-Cooling (TSSG SC) method from the flux using potassium ditungstate (K<sub>2</sub>W<sub>2</sub>O<sub>7</sub>) as a solvent and an undoped [010] oriented seed. The initial Tm<sup>3+</sup> doping level was 1.5 at.% (with respect to Lu<sup>3+</sup>). More details can be found elsewhere [26].

KLu(WO<sub>4</sub>)<sub>2</sub> exhibits a single rare-earth site (Lu<sup>3+</sup>) with  $C_2$  symmetry and VIII-fold oxygen coordination. This compound belongs to the monoclinic class (sp. gr.  $C_2^6_{2h} - C2/c$ ) thus being

optically biaxial. For spectroscopic and laser studies, the crystal was oriented in the frame of the optical indicatrix  $\{N_p, N_m, N_g\}$  following the relation for the principal refractive indices:  $n_p < n_m < n_g$  [30].

## 2.2. ESA spectra

The ESA spectra of  $\text{Tm}^{3+}$  ions were measured by the pump-probe method with polarized light [31]. The spectral resolution was 2.0 nm. Two transitions originating from the metastable  $^3\text{F}_4$   $\text{Tm}^{3+}$  state falling into the near-infrared spectral range were considered,  $^3\text{F}_4 \rightarrow ^3\text{F}_{2,3}$  and  $^3\text{F}_4 \rightarrow ^3\text{H}_4$ , Fig. 2, covering the spectral range of 1–1.6  $\mu\text{m}$ .

The polarized ESA spectra are presented in Fig. 3. The ESA spectra are strongly polarized and the transition cross-sections are relatively high as compared to other oxide and fluoride  $\text{Tm}^{3+}$  doped crystals [31]. In Fig. 3, we also show the ground-state absorption (GSA) and stimulated-emission (SE) cross-section spectra for several 4f transitions of  $\text{Tm}^{3+}$  ions falling into the near-infrared spectral range relevant for the development of 2.3  $\mu\text{m}$  Tm lasers: GSA - the  $^3\text{H}_6 \rightarrow ^3\text{F}_4$ ,  $^3\text{H}_5$  and  $^3\text{H}_4$  transitions, SE - the  $^3\text{H}_4 \rightarrow ^3\text{F}_4$  and  $^3\text{H}_5$  and  $^3\text{F}_4 \rightarrow ^3\text{H}_6$  transitions.

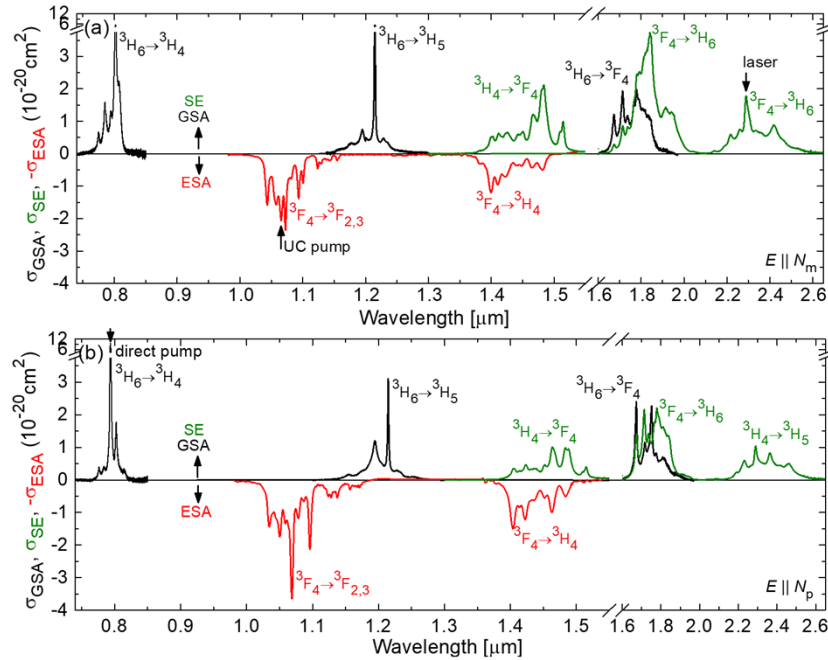


**Fig. 3.** Transition cross-sections of  $\text{Tm}^{3+}$  ions in the monoclinic  $\text{KLu}(\text{WO}_4)_2$  crystal in the short-wave infrared spectral range: (black) GSA,  $\sigma_{\text{GSA}}$ , the  $^3\text{H}_6 \rightarrow ^3\text{F}_4$ ,  $^3\text{H}_5$  and  $^3\text{H}_4$  transitions, (red) ESA,  $\sigma_{\text{ESA}}$ , the  $^3\text{F}_4 \rightarrow ^3\text{F}_{2,3}$  and  $^3\text{F}_4 \rightarrow ^3\text{H}_4$  transitions and (green) SE,  $\sigma_{\text{SE}}$ , the  $^3\text{H}_4 \rightarrow ^3\text{F}_4$  and  $^3\text{H}_5$  and  $^3\text{F}_4 \rightarrow ^3\text{H}_6$  transitions. Light polarizations: (a)  $E \parallel N_m$  and (b)  $E \parallel N_p$ . Arrows indicate the pump and laser wavelengths.

The  $^3\text{F}_4 \rightarrow ^3\text{F}_{2,3}$  ESA transition is of particular interest for demonstrating UC pumping of 2.3  $\mu\text{m}$  Tm lasers employing commercial high-brightness and high-power Yb-fiber lasers emitting slightly above 1  $\mu\text{m}$ . A close look at the ESA spectra in the spectral range addressed by YFLs is shown in Fig. 4. Higher ESA cross-sections are observed for light polarized along the  $N_p$  axis:  $\sigma_{\text{ESA}}$  reaches  $3.57 \times 10^{-20} \text{ cm}^2$  at 1068.7 nm and  $1.69 \times 10^{-20} \text{ cm}^2$  at 1050.3 nm and the peak linewidths (FWHM) are  $\sim 6$  nm and 8 nm, respectively. For light polarized along the  $N_m$ -axis,

$\sigma_{\text{ESA}}$  is  $1.57 \times 10^{-20} \text{ cm}^2$  at 1043.5 nm,  $2.05 \times 10^{-20} \text{ cm}^2$  at 1065.7 nm and  $2.33 \times 10^{-20} \text{ cm}^2$  at 1072.5 nm and the peak linewidths are 7 nm, 8 nm and 5 nm, respectively.

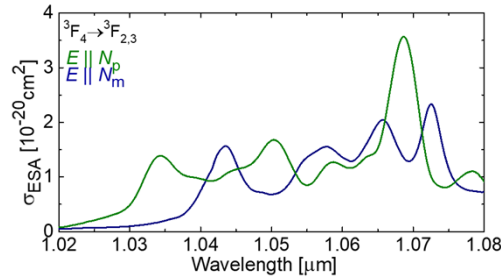


**Fig. 4.** A close look at the  ${}^3\text{F}_4 \rightarrow {}^3\text{F}_{2,3}$  ESA spectra of  $\text{Tm}^{3+}$  ions in  $\text{KLu}(\text{WO}_4)_2$  (the spectral range addressed by Yb-fiber lasers). The light polarizations are  $\mathbf{E} \parallel N_p$  and  $N_m$ .

The  ${}^3\text{F}_4 \rightarrow {}^3\text{H}_4$  ESA transition potentially offers reduced energy losses due to the lack on the NR step from the thermally coupled  ${}^3\text{F}_{2,3}$  states, Fig. 2, however, it is more difficult to address it with high brightness pump sources.  $\text{Tm}^{3+}$  ions can be excited around 1.45  $\mu\text{m}$  using InGaAsP / InP laser diodes. For light polarized along the  $N_p$ -axis,  $\sigma_{\text{ESA}}$  is  $1.00 \times 10^{-20} \text{ cm}^2$  at 1462.8 nm (peak linewidth: 11 nm).

### 3. Laser operation on the ${}^3\text{H}_4 \rightarrow {}^3\text{H}_5$ transition

#### 3.1. Laser set-up

The rectangular laser element was cut from an as-grown 1.5 at.%  $\text{Tm}:\text{KLu}(\text{WO}_4)_2$  crystal (shortly  $\text{Tm}:\text{KLuW}$ , ion density:  $N_{\text{Tm}} = 1.14 \times 10^{20} \text{ at/cm}^2$ ). It was oriented in the optical indicatrix frame with a thickness of 5.97 mm and  $4.10(N_p) \times 3.72(N_m) \text{ mm}^2$  aperture. The crystal orientation for light propagation along the  $N_g$  axis ( $N_g$ -cut) was selected because of the beneficial thermal properties (weak and positive thermal lens) [27], and the access to  $\mathbf{E} \parallel N_p$  and  $\mathbf{E} \parallel N_m$  polarizations corresponding to high absorption / SE cross-sections, Fig. 3. The input/output crystal faces were polished to laser-grade quality with good parallelism and anti-reflection (AR) coated for both used pump wavelengths and the laser one. The laser element was mounted in a water-cooled Cu holder (14 °C) using a silver paint for better heat removal.

The layout of the laser set-up is depicted in Fig. 5. An X-shaped cavity was used. The laser element was placed at normal incidence between two curved (RoC = -100 mm) dichroic folding mirrors  $M_1$  and  $M_2$  coated for high transmission (HT,  $T > 95\%$ ) at 0.79 and 1.06  $\mu\text{m}$  and for high reflection (HR) at 2.18–2.35  $\mu\text{m}$ . One cavity arm contained a plane HR rear mirror, and the other arm was terminated by a plane-wedged output coupler (OC) with a transmission  $T_{\text{OC}}$  in the range of 0.5% - 4% at 2.3  $\mu\text{m}$ . All the cavity mirrors except of the OC also provided HT ( $T > 90\%$ ) at 1.9  $\mu\text{m}$  to suppress competitive oscillations on the  ${}^3\text{F}_4 \rightarrow {}^3\text{H}_6$  transition. The calculated diameter of the laser mode in the crystal was 68 / 82  $\mu\text{m}$  in the sagittal / tangential planes.

Two pump sources were used. The first one was a Ti:Sapphire laser (3900S, Spectra Physics) delivering up to 3.3 W at 793.6 nm (laser linewidth: 0.1 nm) with linear polarization and nearly diffraction limited beam quality ( $M^2 \approx 1$ ). It addressed the  ${}^3\text{H}_6 \rightarrow {}^3\text{H}_4$  GSA transition of  $\text{Tm}^{3+}$  ions (direct pumping). The second pump source was a commercial Yb fiber laser (CYFL-TERA series, Keopsys) emitting up to 10 W at 1064 nm (laser linewidth: < 2 nm) addressing the  ${}^3\text{F}_4 \rightarrow {}^3\text{F}_{2,3}$  ESA  $\text{Tm}^{3+}$  transition (UC pumping). Crossed-polarization pumping was used: the polarization of the direct and UC pump radiation was aligned to be  $\mathbf{E} \parallel N_p$  and  $\mathbf{E} \parallel N_m$ , respectively, in the laser crystal. The two pump beams were combined using a flat dichroic mirror (DM) installed at 45° and coated for HT at 0.79  $\mu\text{m}$  and HR at 1.06  $\mu\text{m}$ . The pump radiation was

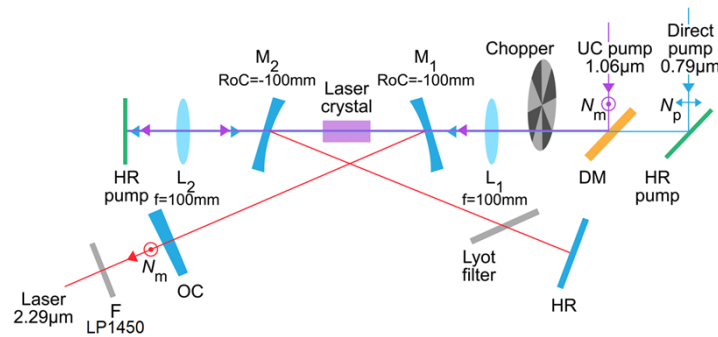


**Fig. 5.** Scheme of 2.3  $\mu\text{m}$  Tm laser:  $M_1$ ,  $M_2$  – curved pump mirrors, HR – flat rear mirror, OC – plane-wedged output coupler,  $L_1$  and  $L_2$  – aspherical lenses, DM – dichroic mirror (pump combiner), HR pump – highly-reflective mirrors for the pump radiation, F – long-pass filter.

focused into the laser crystal through the  $M_1$  mirror using an AR-coated aspherical lens (focal length:  $f = 100$  mm). Due to the relatively weak single-pass pump absorption, the non-absorbed pump was recirculated using another lens  $L_2$  ( $f = 100$  mm) and a plane HR mirror placed behind the  $M_2$  cavity mirror. To well match the radii of the two pump beams in the crystal, two telescopes were implemented. The resulting pump spot diameter for both pump beams was  $70 \pm 10$   $\mu\text{m}$ . An optical isolator was used to protect the Yb fiber laser from back reflections. Under pure UC pumping, the pump beam was modulated with a mechanical chopper (duty cycle: 1:6, pulse duration:  $\sim 10$  ms) to reduce the heat loading in the laser crystal.

For wavelength tuning, we used an uncoated 2 mm-thick quartz birefringent plate (BIR1020, Newlight Photonics). The optical axis ( $c$ -axis) was lying in the plane of the plate. The plate was placed at the Brewster's angle in the cavity arm terminated by the HR mirror.

The residual pump after the OC was filtered out using a long-pass filter (LP1450, Spectrogon). The laser spectra were measured using an optical spectrum analyzer (AQ6375B, Yokogawa; resolution, 0.2 nm). The polarization state of the laser emission was determined using a Glan-Taylor polarizer.

### 3.2. Pure direct pumping

At first, we studied pure direct pumping at 0.79  $\mu\text{m}$  (the  ${}^3\text{H}_6 \rightarrow {}^3\text{H}_4$  GSA transition). The Tm laser generated a maximum CW output power of 813 mW at 2291 nm with a slope efficiency  $\eta$  of 44.7% (vs. the incident pump power) and a laser threshold of 0.819 W (for an output coupling  $T_{\text{OC}} = 3\%$ ), Fig. 6(a). The optical efficiency  $\eta_{\text{opt}}$  was then 26.9%. With increasing  $T_{\text{OC}}$ , the laser threshold gradually increased, from 0.391 W ( $T_{\text{OC}} = 0.5\%$ ) up to 0.956 W ( $T_{\text{OC}} = 4\%$ ). The input-output power dependences were nonlinear near the laser threshold.

The typical spectra of laser emission are shown in Fig. 6(b), measured well above the laser threshold. As expected for a quasi-four-level  ${}^3\text{H}_4 \rightarrow {}^3\text{H}_5$  laser transition, they were weakly dependent on the output coupling and a single laser line was observed at 2291 nm (laser linewidth: 1.0 nm). No parasitic colasing on the  ${}^3\text{F}_4 \rightarrow {}^3\text{H}_6$  transition was observed.

The total (double-pass) pump absorption in the crystal under non-lasing and lasing (for  $T_{\text{OC}} = 0.5\%$ ) conditions was studied, Fig. 6(c). In the former case, it gradually decreased with the incident pump power representing ground-state ( ${}^3\text{H}_6$ ) bleaching. Under lasing conditions, the pump absorption was nearly clamped above the laser threshold and only a weak saturation was observed due to accumulation of electronic excitations in the metastable intermediate  ${}^3\text{F}_4$  Tm $^{3+}$  manifold.

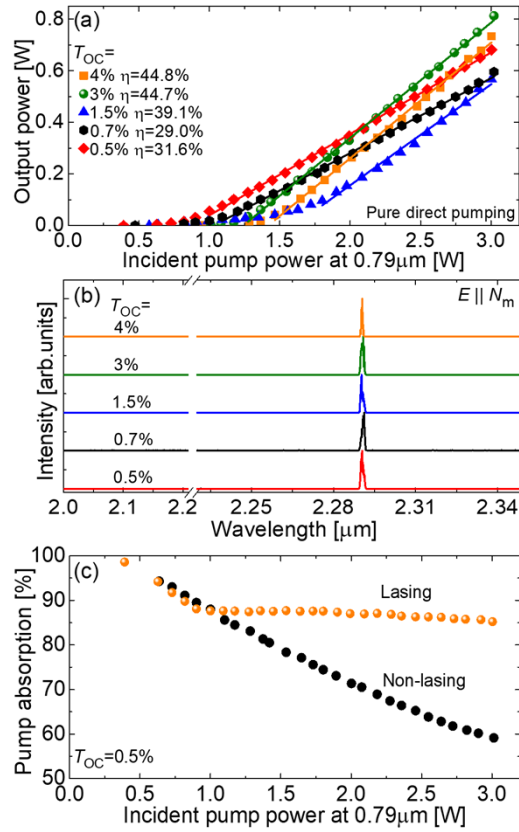


**Fig. 6.** 2.3 μm Tm laser with a pure direct pumping at 0.79 μm (the  ${}^3\text{H}_6 \rightarrow {}^3\text{H}_4$  GSA transition): (a) input-output dependences,  $\eta$  – slope efficiency; (b) typical spectra of laser emission measured well above the laser threshold, laser polarization:  $E \parallel N_m$ ; (c) total (double-pass) pump absorption under non-lasing and lasing (for  $T_{OC} = 0.5\%$ ) conditions.

### 3.3. Dual-wavelength pumping

Then, dual-wavelength pumping at 0.79 and 1.06 μm was studied in the CW regime. In the first experiment, the pump power  $P_{0.79\mu\text{m}}$  was fixed and  $P_{1.06\mu\text{m}}$  was varied, see Fig. 7(a). Although certain power scaling was achieved in this way, the effect was relatively weak, e.g., for  $P_{0.79\mu\text{m}} = 1.87$  W, by increasing  $P_{1.06\mu\text{m}}$  from 0 to 2.56 W, the output power of the Tm laser increased almost linearly from 308 to 383 mW (for  $T_{OC} = 0.5\%$ ), so that the total optical efficiency of the laser (vs. the total incident pump power)  $\eta_{\text{opt},\Sigma}$  dropped from 16.5% to 8.6%.

The relative increase of the output power of the Tm laser operating on the  ${}^3\text{H}_4 \rightarrow {}^3\text{H}_5$  transition under dual-wavelength pumping was more profound near the laser threshold, as seen in Fig. 7(b). Under pure direct pumping, the laser generated 670 mW at 2291 nm with  $\eta_{\text{opt}} = 22.2\%$  and a threshold of 0.219 W. By adding UC pumping with  $P_{1.06\mu\text{m}} = 2.06$  W, the laser generated a very similar output power of 672 mW with a reduced  $\eta_{\text{opt},\Sigma}$  of 13.2%. As for the laser threshold, it decreased in terms of pump power at 0.79 μm (to 0.200 W) while increased in terms of the total incident pump power (up to 2.26 W).

To better understand the threshold laser behavior and the possible benefits of the dual-wave pumping, we systematically studied the laser threshold as a function of different combinations of  $P_{0.79\mu\text{m}}$  and  $P_{1.06\mu\text{m}}$  pump powers, Fig. 7(c). By increasing the co-pumping at 0.79 μm, the power at 1.06 μm needed to reach the threshold gradually decreased. Even a small addition of

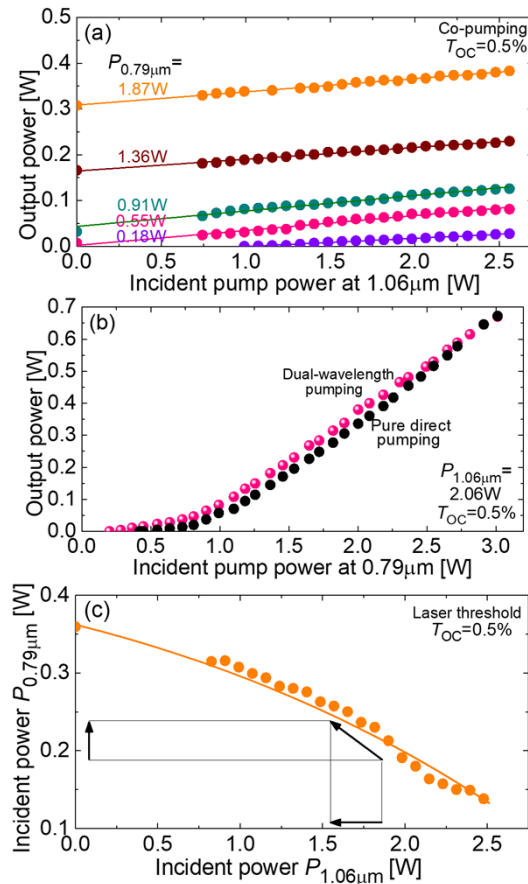


**Fig. 7.** 2.3 μm Tm laser with a cross-polarization dual-wavelength pumping at 0.79 μm and 1.06 μm (the  ${}^3\text{H}_6 \rightarrow {}^3\text{H}_4$  GSA and  ${}^3\text{F}_4 \rightarrow {}^3\text{F}_{2,3}$  ESA transitions): (a) output power vs. the incident pump power at 1.06 μm for fixed seeding pump powers at 0.79 μm; (b) input-output dependences for  $T_{OC} = 0.5\%$ : pure and dual-wavelength pumping; (c) laser threshold as a function of the incident pump power at both pump wavelengths,  $T_{OC} = 0.5\%$ .

direct pumping resulted in a great benefit in reducing  $P_{1.06\mu m}$ . This is explained by the seeding effect of the direct pump on the population of the intermediate long-living  ${}^3\text{F}_4$   $\text{Tm}^{3+}$  level which acts as an efficient ground-state for the resonant  ${}^3\text{F}_4 \rightarrow {}^3\text{F}_{2,3}$  ESA process [32].

At low UC pump powers, the seeding effect of even a weak direct pump is essential to boost the pump absorption at 1.06 μm leading to a drop of the laser threshold in terms of the incident pump power. At high pump levels, the absorption at 1.06 μm is saturated owing to the photon avalanche effect. Consequently, the main benefit of dual-wavelength pumping can be formulated as follows: when using a high-power Yb-fiber laser as a primary pump source for Tm lasers operating on the  ${}^3\text{H}_4 \rightarrow {}^3\text{H}_5$  transition, a low-power co-pumping at 0.79 μm (e.g., by spatially single-mode fiber-coupled AlGaAs diode lasers) can reduce the laser threshold for UC pumping which could be of great importance, e.g., for designing mode-locked lasers.

### 3.4. Pure upconversion pumping

Then, we studied pure UC pumping at  $1.06\ \mu\text{m}$  (the  ${}^3\text{F}_4 \rightarrow {}^3\text{F}_{2,3}$  ESA transition). To reduce the heat loading in the crystal and the risk of its thermal fracture, the experiment was performed in the quasi-CW regime (duty cycle: 1:6).

The Tm laser operating on the  ${}^3\text{H}_4 \rightarrow {}^3\text{H}_5$  transition generated a maximum peak output power of 433 mW at 2291 nm with a slope efficiency  $\eta$  of 7.4% (for high  $T_{\text{OC}} = 4\%$ ), see Fig. 8(a). This corresponded to an optical efficiency  $\eta_{\text{opt}}$  of 4.7% (at the maximum incident pump power of 9.25 W). The laser threshold decreased for smaller output coupling, from 3.19 W ( $T_{\text{OC}} = 4\%$ ) down to 2.14 W ( $T_{\text{OC}} = 0.5\%$ ). This experiment corresponded to a slightly different cavity configuration leading to a lower threshold for UC pumping (as compared to Section 4.3). The input-output dependences were linear.

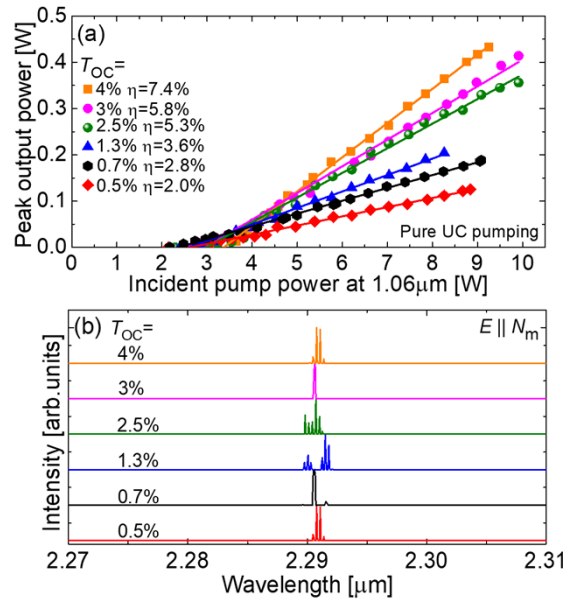


**Fig. 8.**  $2.3\ \mu\text{m}$  Tm laser with a pure upconversion pumping at  $1.06\ \mu\text{m}$  (the  ${}^3\text{F}_4 \rightarrow {}^3\text{F}_{2,3}$  ESA transition): (a) input-output dependences,  $\eta$  – slope efficiency, quasi-CW operation, duty cycle: 1:6; (b) laser spectra measured well above the laser threshold, laser polarization:  $E \parallel N_m$ .

The spectra of laser emission under pure UC pumping are presented in Fig. 8(b). The Tm laser operated at  $\sim 2.29\ \mu\text{m}$  and the spectra were almost independent on the transmission of the output coupler. Still, they were slightly broader than in the case of pure direct pumping, compare with Fig. 6(b). Again, no colasing on the  ${}^3\text{F}_4 \rightarrow {}^3\text{H}_6$  transition was observed.

The characteristics of the Tm laser operating solely on the  ${}^3\text{H}_4 \rightarrow {}^3\text{H}_5$  transition with a pure UC pumping at  $1.06\ \mu\text{m}$  were numerically simulated using a rate-equation model based on the determined spectroscopic parameters and the utilized cavity design (see above). The pump absorption under single- and double-pass pumping as a function of the incident pump power at  $1.06\ \mu\text{m}$  is shown in Fig. 9(a). It gradually increases at small pump powers and then saturates representing an equilibrium in recirculating the populations of the  ${}^3\text{H}_6$ ,  ${}^3\text{F}_4$  and  ${}^3\text{H}_4$  Tm $^{3+}$  levels via the photon avalanche mechanism. For double-pass pumping, the pump absorption is higher (saturated value:  $22.3 \pm 0.4\%$ ) and its saturation occurs faster. Thus, the highest slope efficiency of the developed Tm laser with respect to the absorbed pump power was 33.2%, representing the

best result for any bulk Tm laser operating solely on the  ${}^3\text{H}_4 \rightarrow {}^3\text{H}_5$  transition with a pure UC pumping and approaching the value achieved for a Tm-fiber laser [25].

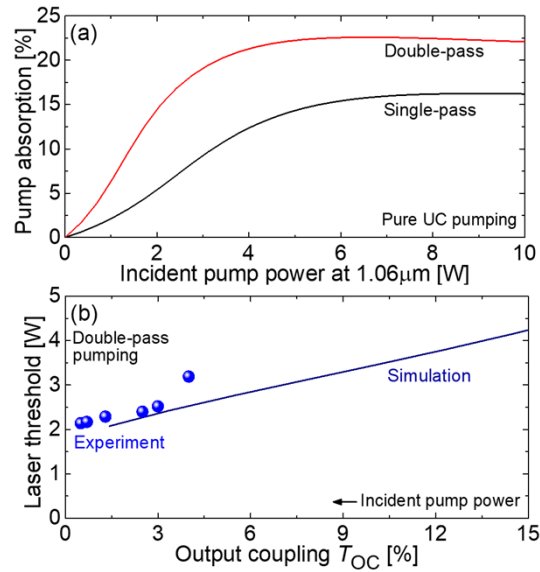


**Fig. 9.** Numerical simulations of (a) the pump absorption (single- and double-pass pumping) and (b) the laser threshold (under double-pass pumping) as a function of the output coupler transmission for a Tm laser operating on the  ${}^3\text{H}_4 \rightarrow {}^3\text{H}_5$  transition with a pure UC pumping at 1.06 μm. In (b), the experimental data on the laser thresholds (incident pump power) are shown as circles.

The laser threshold of the Tm laser was also simulated showing a reasonable agreement with the experiment, Fig. 9(b). As expected, it gradually increased with the output coupling.

### 3.5. Wavelength tuning

The broadband emission properties of  $\text{Tm}^{3+}$  ions around 2.3 μm in the studied tungstate crystal motivated us to study the wavelength tuning performance of this material. The Lyot filter was inserted at Brewster's angle in the cavity arm terminated by the plane rear mirror. A small output coupling  $T_{OC} = 0.5\%$  was used and the incident pump power  $P_{0.79\mu\text{m}}$  was 2.9 W.

The obtained tuning curve is shown in Fig. 10. The laser wavelength was continuously tuned over two wavelength ranges: 2256–2345 nm (tuning range: 90 nm at the zero-power level) and 2387–2422 nm (tuning range: 35 nm). The maximum in the tuning curve was observed at 2291 nm (output power: 454 mW), in agreement with the luminescence spectrum and the free-running laser spectrum. The high insertion loss of the Lyot filter probably originated from its weak residual absorption at these wavelengths. The laser polarization was linear,  $E \parallel N_m$ .

The wavelength tuning experiment indicated the high potential of the Tm:KLuW crystal for the development of femtosecond ML lasers at 2.3 μm. Indeed, the emission bandwidth of the peak at 2291 nm is 32 nm (FWHM). We report on the first lasing from this material at 2.4 μm. Further power scaling at this wavelength is expected with spectrally selective (long-pass) cavity mirrors. This second spectral range is also attractive for ML laser development, as the emission bandwidth of the peak centered at 2420 nm is as broad as 76 nm.

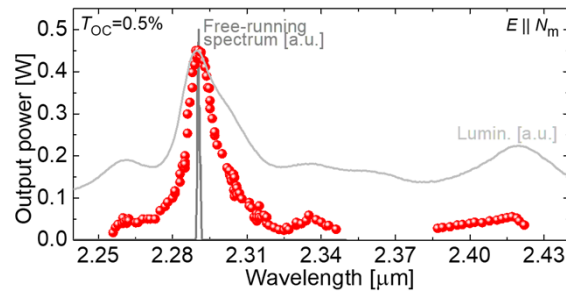


**Fig. 10.** Wavelength tuning curve for a Tm laser operating on the  ${}^3\text{H}_4 \rightarrow {}^3\text{H}_5$  transition with a pure direct pumping at  $0.79\ \mu\text{m}$ , light grey curve – luminescence spectrum, dark grey curve – free-running laser spectrum,  $P_{0.79\mu\text{m}} = 2.9\ \text{W}$ ,  $T_{\text{OC}} = 0.5\%$ , laser polarization:  $E \parallel N_m$ .

#### 4. Conclusions

To conclude, upconversion pumping of thulium lasers operating on the  ${}^3\text{H}_4 \rightarrow {}^3\text{H}_5$  transition using commercial high-brightness and power scalable Yb-fiber lasers emitting slightly above  $1\ \mu\text{m}$  (thus addressing the  ${}^3\text{F}_4 \rightarrow {}^3\text{F}_{2,3}$  excited-state absorption transition of  $\text{Tm}^{3+}$  ions) appears as a viable route towards generating laser emission at  $2.3\ \mu\text{m}$ , in the spectral range containing multiple absorption lines of several molecular species, cf. Figure 1. This pump scheme is particularly attractive for pumping mode-locked  $2.3\ \mu\text{m}$  thulium lasers.

The major issue of pure UC pumping consists of reaching reasonably high pump absorption in the gain medium. It can be overcome by (i) using a wavelength tunable pump source, (ii) employing anisotropic gain media with high ESA transition cross-sections (such as monoclinic double tungstate crystals), (iii) optimizing the  $\text{Tm}^{3+}$  doping level or (iv) using co-pumping at  $0.79\ \mu\text{m}$  to populate the  ${}^3\text{F}_4$   $\text{Tm}^{3+}$  intermediate long-living level thus boosting the ESA efficiency from this manifold. The latter seems feasible with low to moderate power fiber-coupled AlGaAs laser diodes emitting at  $0.79\ \mu\text{m}$ .

Monoclinic potassium lutetium double tungstate doped with  $\text{Tm}^{3+}$  ions is an attractive gain medium for UC pumped lasers operating on the  ${}^3\text{H}_4 \rightarrow {}^3\text{H}_5$  transition owing to its exceptionally high ESA cross-sections for polarized light around  $1\ \mu\text{m}$ . By using a commercial  $1064\ \text{nm}$  Yb-fiber laser to pump this crystal, we obtained a record-high output power from any UC pumped bulk  $2.3\ \mu\text{m}$  Tm-laser, namely  $433\ \text{mW}$  at  $2291\ \text{nm}$  corresponding to a linearly polarized laser emission. Further power scaling seems feasible by optimizing the  $\text{Tm}^{3+}$  doping level and better addressing the ESA peaks.

The wavelength tuning experiment indicated a high potential of this material for generation of femtosecond laser pulses around  $2.3$  and  $2.4\ \mu\text{m}$ .

**Funding.** Ministerio de Ciencia e Innovación (PID2019-108543RB-I00); European Commission (Operational Program ERDF/ESF 2014–2020); Agence Nationale de la Recherche (ANR-10-LABX-09-01, ANR-19-CE08-0028).

**Acknowledgments.** Mateos acknowledges the Serra Hünter program.

**Disclosures.** The authors declare no conflicts of interest.

**Data availability.** Data underlying the results presented in this paper are not publicly available at this time but may be obtained from the authors upon reasonable request.

#### References

1. J. Koetke and G. Huber, "Infrared excited-state absorption and stimulated-emission cross sections of  $\text{Er}^{3+}$ -doped crystals," *Appl. Phys. B* **61**(2), 151–158 (1995).
2. N. Garnier, R. Moncorgé, H. Manaa, E. Descroix, P. Laporte, and Y. Guyot, "Excited-state absorption of  $\text{Tm}^{3+}$ -doped single crystals at photon-avalanche wavelengths," *J. Appl. Phys.* **79**(8), 4323–4329 (1996).

3. H. Scheife, G. Huber, E. Heumann, S. Bär, and E. Osiać, "Advances in up-conversion lasers based on  $\text{Er}^{3+}$  and  $\text{Pr}^{3+}$ ," *Opt. Mater.* **26**(4), 365–374 (2004).
4. S. A. Pollack, D. B. Chang, and N. L. Moise, "Upconversion-pumped infrared erbium laser," *J. Appl. Phys.* **60**(12), 4077–4086 (1986).
5. T. Hebert, R. Wannemacher, R.M. Macfarlane, and W. Lenth, "Blue continuously pumped upconversion lasing in  $\text{Tm}:\text{YLiF}_4$ ," *Appl. Phys. Lett.* **60**(21), 2592–2594 (1992).
6. F. Heine, E. Heumann, T. Danger, T. Schweizer, G. Huber, and B. Chai, "Green upconversion continuous wave  $\text{Er}^{3+}:\text{LiYF}_4$  laser at room temperature," *Appl. Phys. Lett.* **65**(4), 383–384 (1994).
7. R. M. Macfarlane, F. Tong, A. J. Silversmith, and W. Lenth, "Violet cw neodymium upconversion laser," *Appl. Phys. Lett.* **52**(16), 1300–1302 (1988).
8. T. Komukai, T. Yamamoto, T. Sugawa, and Y. Miyajima, "Upconversion pumped thulium-doped fluoride fiber amplifier and laser operating at 1.47  $\mu\text{m}$ ," *IEEE J. Quantum Electron.* **31**(11), 1880–1889 (1995).
9. H. M. Pask, A. C. Tropper, and D. C. Hanna, "A  $\text{Pr}^{3+}$ -doped ZBLAN fibre upconversion laser pumped by an  $\text{Yb}^{3+}$ -doped silica fibre laser," *Opt. Commun.* **134**(1-6), 139–144 (1997).
10. M. Schellhorn, "High-power diode-pumped  $\text{Tm}:\text{YLF}$  laser," *Appl. Phys. B* **91**(1), 71–74 (2008).
11. E. C. Honea, R. J. Beach, S. B. Sutton, J. A. Speth, S. C. Mitchell, J. A. Skidmore, M. A. Emanuel, and S. A. Payne, "115-W  $\text{Tm}:\text{YAG}$  diode-pumped solid-state laser," *IEEE J. Quantum Electron.* **33**(9), 1592–1600 (1997).
12. J. F. Pinto, L. Esterowitz, and G. H. Rosenblatt, " $\text{Tm}^{3+}:\text{YLF}$  laser continuously tunable between 2.20 and 2.46  $\mu\text{m}$ ," *Opt. Lett.* **19**(12), 883–885 (1994).
13. I. E. Gordon, L. S. Rothman, R. J. Hargreaves, R. Hashemi, E. V. Karlovets, F. M. Skinner, E. K. Conway, C. Hill, R. V. Kochanov, Y. Tan, and P. Wcislo, "The HITRAN2020 molecular spectroscopic database," *J. Quant. Spectrosc. Radiat. Transfer* **277**, 107949 (2022).
14. P. Loiko, R. Soulard, L. Guillemot, G. Brasse, J.L. Doualan, A. Braud, A. Tyazhev, A. Hideur, F. Druon, and P. Camy, "Efficient  $\text{Tm}:\text{LiYF}_4$  lasers at 2.3  $\mu\text{m}$ : Effect of energy-transfer upconversion," *IEEE J. Quantum Electron.* **55**(6), 1700212 (2019).
15. L. Guillemot, P. Loiko, A. Braud, J.-L. Doualan, A. Hideur, M. Koselja, R. Moncorgé, and P. Camy, "Continuous-wave  $\text{Tm}:\text{YAIO}_3$  laser at  $\sim 2.3$   $\mu\text{m}$ ," *Opt. Lett.* **44**(20), 5077–5080 (2019).
16. L. Guillemot, P. Loiko, E. Kifle, J.-L. Doualan, A. Braud, F. Starecki, T. Georges, J. Rouvillain, A. Hideur, and P. Camy, "Watt-level mid-infrared continuous-wave  $\text{Tm}:\text{YAG}$  laser operating on the  $^3\text{H}_4 \rightarrow ^3\text{H}_5$  transition," *Opt. Mater.* **101**, 109745 (2020).
17. L. Guillemot, P. Loiko, R. Soulard, A. Braud, J.L. Doualan, A. Hideur, and P. Camy, "Close look on cubic  $\text{Tm}:\text{KY}_3\text{F}_{10}$  crystal for highly efficient lasing on the  $^3\text{H}_4 \rightarrow ^3\text{H}_5$  transition," *Opt. Express* **28**(3), 3451–3463 (2020).
18. Ò. Silvestre, M. C. Pujol, M. Rico, F. Güell, M. Aguiló, and F. Díaz, "Thulium doped monoclinic  $\text{KLu}(\text{WO}_4)_2$  single crystals: growth and spectroscopy," *Appl. Phys. B* **87**(4), 707–716 (2007).
19. L. Guillemot, P. Loiko, R. Soulard, A. Braud, J.L. Doualan, A. Hideur, R. Moncorgé, and P. Camy, "Thulium laser at  $\sim 2.3$   $\mu\text{m}$  based on upconversion pumping," *Opt. Lett.* **44**(16), 4071–4074 (2019).
20. M. F. Joubert, S. Guy, B. Jacquier, and C. Linares, "The photon-avalanche effect: review, model and application," *Opt. Mater.* **4**(1), 43–49 (1994).
21. R. Soulard, A. Tyazhev, J.-L. Doualan, A. Braud, A. Hideur, M. Laroche, B. Xu, and P. Camy, "2.3  $\mu\text{m}$   $\text{Tm}^{3+}:\text{YLF}$  mode-locked laser," *Opt. Lett.* **42**(18), 3534–3536 (2017).
22. F. Canbaz, I. Yorulmaz, and A. Sennaroglu, "Kerr-lens mode-locked 2.3- $\mu\text{m}$   $\text{Tm}^{3+}:\text{YLF}$  laser as a source of femtosecond pulses in the mid-infrared," *Opt. Lett.* **42**(19), 3964–3967 (2017).
23. Y. Morova, M. Tonelli, V. Petrov, and A. Sennaroglu, "Upconversion pumping of a 2.3  $\mu\text{m}$   $\text{Tm}^{3+}:\text{KY}_3\text{F}_{10}$  laser with a 1064 nm ytterbium fiber laser," *Opt. Lett.* **45**(4), 931–934 (2020).
24. R. M. El-Agmy and N. M. Al-Hosiny, "2.31  $\mu\text{m}$  laser under up-conversion pumping at 1.064  $\mu\text{m}$  in  $\text{Tm}^{3+}:\text{ZBLAN}$  fibre lasers," *Electron. Lett.* **46**(13), 936–937 (2010).
25. A. Tyazhev, F. Starecki, S. Cozic, P. Loiko, L. Guillemot, A. Braud, F. Joulain, M. Tang, T. Godin, A. Hideur, and P. Camy, "Watt-level efficient 2.3  $\mu\text{m}$  thulium fluoride fiber laser," *Opt. Lett.* **45**(20), 5788–5791 (2020).
26. V. Petrov, M. C. Pujol, X. Mateos, Ò. Silvestre, S. Rivier, M. Aguiló, R. M. Solé, J. Liu, U. Griebner, and F. Díaz, "Growth and properties of  $\text{KLu}(\text{WO}_4)_2$ , and novel ytterbium and thulium lasers based on this monoclinic crystalline host," *Laser Photonics Rev.* **1**(2), 179–212 (2007).
27. J. M. Serres, X. Mateos, P. Loiko, K. Yumashev, N. Kuleshov, V. Petrov, U. Griebner, M. Aguiló, and F. Díaz, "Diode-pumped microchip  $\text{Tm}:\text{KLu}(\text{WO}_4)_2$  laser with more than 3 W of output power," *Opt. Lett.* **39**(14), 4247–4250 (2014).
28. P. Loiko, J. M. Serres, X. Mateos, K. Yumashev, A. Yasukevich, V. Petrov, U. Griebner, M. Aguiló, and F. Díaz, "Subnanosecond  $\text{Tm}:\text{KLuW}$  microchip laser Q-switched by a  $\text{Cr}:\text{ZnS}$  saturable absorber," *Opt. Lett.* **40**(22), 5220–5223 (2015).
29. A. Schmidt, S. Y. Choi, D. I. Yeom, F. Rotermund, X. Mateos, M. Segura, F. Diaz, V. Petrov, and U. Griebner, "Femtosecond pulses near 2  $\mu\text{m}$  from a  $\text{Tm}:\text{KLuW}$  laser mode-locked by a single-walled carbon nanotube saturable absorber," *Appl. Phys. Express* **5**(9), 092704 (2012).
30. P. Loiko, P. Segonds, P. L. Inácio, A. Peña, J. Debray, D. Rytz, V. Filippov, K. Yumashev, M. C. Pujol, X. Mateos, M. Aguiló, F. Díaz, M. Eichhorn, and B. Boulanger, "Refined orientation of the optical axes as a function of wavelength

- in three monoclinic double tungstate crystals  $\text{KRE}(\text{WO}_4)_2$  ( $\text{RE} = \text{Gd}, \text{Y}$  or  $\text{Lu}$ ),” *Opt. Mater. Express* **6**(9), 2984–2990 (2016).
31. L. Guillemot, P. Loiko, J.-L. Doualan, A. Braud, and P. Camy, “Excited-state absorption in thulium-doped materials in the near-infrared,” *Opt. Express* **30**(18), 31669–31684 (2022).
  32. H. Dupont, L. Guillemot, P. Loiko, A. Braud, J.-L. Doualan, P. Camy, P. Georges, and F. Druon, “Dual-wavelength-pumping of mid-infrared Tm:YLF laser at 2.3  $\mu\text{m}$ : demonstration of pump seeding and recycling processes,” *Opt. Express* **30**(18), 32141–32150 (2022).